A&A 679, A151 (2023)
https://doi.org/10.1051/0004-6361/202347392

Astronomy & Astrophysics

Link between star formation and the properties of supermassive black holes

George Mountrichas[1] and Véronique Buat[2,3]

[1] Instituto de Fisica de Cantabria (CSIC-Universidad de Cantabria), Avenida de los Castros, 39005 Santander, Spain
e-mail: gmountrichas@gmail.com
[2] Aix-Marseille Univ., CNRS, CNES, LAM, Marseille, France
[3] Institut Universitaire de France (IUF), Marseille, France

Received 7 July 2023 / Accepted 27 September 2023

ABSTRACT

It is well known that supermassive black holes (SMBHs) and their host galaxies undergo a process of co-evolution. Feedback from active galactic nuclei (AGNs) plays an important role in this symbiosis. To study the effect of AGN feedback on the host galaxy, one popular method is to study the star formation rate (SFR) as a function of the X-ray luminosity (L_X). However, hydrodynamical simulations suggest that the cumulative impact of AGN feedback on a galaxy is encapsulated in the mass of the SMBH, M_{BH}, rather than the L_X. In this study, we compare the SFRs of AGN and non-AGN galaxies as a function of L_X, M_{BH}, the Eddington ratio (n_{Edd}), and the specific black hole accretion rate (λ_{sBHAR}). For that purpose, we used 122 X-ray AGN in the XMM-XXL field and 3371 galaxies from the VIPERS survey to calculate the SFR_{norm} parameter, defined as the ratio of the SFR of AGN to the SFR of non-AGN galaxies with similar stellar mass, M_*, and redshift. Our datasets span a redshift range of $0.5 \leq z \leq 1.2$. The results show that the correlation between SFR_{norm} and M_{BH} is stronger compared to that between SFR_{norm} and L_X. A weaker correlation is found between SFR_{norm} and λ_{sBHAR}. No correlation is detected between SFR_{norm} and n_{Edd}. These results corroborate the notion that the M_{BH} is a more robust tracer of the cumulative impact of the AGN feedback, compared to the instantaneous accretion rate (L_X). Thus, it may serve as a better predictive parameter of changes in the SFR of the host galaxy.

Key words. galaxies: active – galaxies: evolution – galaxies: star formation – X-rays: galaxies – X-rays: general

1. Introduction

The supermassive black holes (SMBHs) that live in the centre of galaxies become active when material that is in the vicinity of the SMBH is accreted onto them. A great deal of evidence presented over the past two decades has shown that a co-evolution between the SMBH and its host galaxy exists. For instance, both the activity of the black hole and the star formation (SF) of galaxies are fed by the same material (i.e., cold gas) and both phenomena peak at about the same cosmic time ($z \sim 2$; e.g., Boyle et al. 2000; Sobral et al. 2013). Moreover, tight correlations have been found in the Local Universe, between the mass of the SMBH, M_{BH}, and various properties of the host galaxy, such as the stellar velocity dispersion the bulge luminosity and the bulge mass (e.g., Magorrian et al. 1998; Ferrarese & Merritt 2000; Tremaine et al. 2002; Häring & Rix 2004). These correlations also seem to exist at higher redshifts ($z \sim 2$; e.g., Jahnke et al. 2009; Merloni et al. 2010; Sun et al. 2015; Suh et al. 2020; Setoguchi et al. 2021; Mountrichas 2023).

Various mechanisms have been suggested that drive the gas from kiloparsec to sub-parsec scales (for a review see Alexander & Hickox 2012). Also, AGN feedback in the form of jets, radiation, or winds has been included in most simulations to explain many galaxy properties, with respect to the way the hot intracluster medium is maintained (e.g., Dunn & Fabian 2006), the shape of the galaxy stellar mass function is formed (e.g., Bower et al. 2012), and the galaxy morphology is composed (e.g., Dubois et al. 2016).

A popular method to study the symbiosis between the AGN and its host galaxy is to examine the correlation between the star formation rate (SFR) and the power of AGN, using the X-ray luminosity (L_X) as a proxy for the latter. Most prior studies have found a positive correlation between the SFR and L_X (e.g., Lanzuisi et al. 2017; Masoura et al. 2018; Brown et al. 2019), whereas no specific correlation was reported in Stanley et al. (2015). However, more information can be gained when we compare the SFR of AGN with the SFR of non-AGN galaxies with similar redshifts and stellar masses, M_*, as a function of L_X (e.g., Santini et al. 2012; Shimizu et al. 2015, 2017; Florez et al. 2020). In this case, most studies measure what is often call normalized SFR, namely, SFR_{norm}, which is the ratio of AGN to the ratio of SF main-sequence (MS) galaxies with similar redshift and M_* (Rosario et al. 2013; Mullaney et al. 2015; Bernhard et al. 2019). A strong positive correlation has been found between SFR_{norm} and L_X at redshifts of up to $z \sim 5$ (Masoura et al. 2021; Koutoulidis et al. 2022; Pouliasis et al. 2022). However, after minimizing systematics effects that may be introduced in the comparison of the SFR of AGN and non-AGN systems (e.g., due to the different methods used to calculate the SFR of the two populations, the different photometric selection criteria that have been applied; for more details, see Mountrichas et al. 2021c), a weaker correlation or even the absence of any correlation is detected between SFR_{norm} and L_X, depending on the M_* range (see Fig. 5 in Mountrichas et al. 2022a).

The different trends observed in the $SFR_{norm}-L_X$ relation in different M_* regimes, also highlight the importance of M_* in

this kind of investigations. There are observational works that have found that the black hole accretion rate (BHAR $\propto L_X$) is mainly linked to M_* rather than SFR (Yang et al. 2017). Moreover, SFR_{norm} appears to be stronger correlated with M_* than with L_X (Mountrichas et al. 2022a). Theoretical studies that used hydrodynamical simulations have also found that that the cumulative impact of AGN feedback on the host galaxy is encapsulated in the mass of the supermassive black hole, M_{BH}, and not in L_X, both in the Local Universe (Piotrowska et al. 2022) and at high redshifts (Bluck et al. 2023). The fact that the SFR shows a strong link both with M_* and M_{BH} could be due to the underlying M_*-M_{BH} relation that has been found to hold up to at least redshift of 2 (e.g., Merloni et al. 2010; Sun et al. 2015; Setoguchi et al. 2021; Mountrichas 2023).

In this work, we compare the SFR of X-ray detected AGN with that of non-AGN galaxies as a function of different black hole properties. For that purpose, we use X-ray AGN detected in the XMM-XXL field, for which there are available M_{BH} measurements, and a sample of (non-AGN) galaxies from the VIPERS survey that (partially) overlaps with XMM-XXL. We use these two samples to calculate the SFR_{norm} parameter and examine the correlation of SFR_{norm} with the L_X, M_{BH}, Eddington ratio (n_{Edd}), and specific black hole accretion rate (λ_{sBHAR}). Finally, we discuss our results and describe our main conclusions. Throughout this work, we assume a flat ΛCDM cosmology with $H_0 = 70.4\,km\,s^{-1}\,Mpc^{-1}$ and $\Omega_M = 0.272$ (Komatsu et al. 2011).

2. Data

The main goal of this study is to examine how the SFR of X-ray AGN compares with the SFR of non-AGN systems as a function of various black hole properties. For that purpose, we compiled an X-ray dataset that comprises of AGN detected in the XMM-XXL field and a control sample of (non-AGN) galaxies made up of sources observed by the VIPERS survey. The sky area that the two surveys cover (partially) overlaps. Below, we provide a brief description of these two surveys. The (final) AGN and non-AGN samples used in our analysis are described in Sect. 4.

2.1. The XMM-XXL dataset

The X-ray dataset used in this work consists of X-ray AGN observed in the northern field of the *XMM-Newton*-XXL survey (XMM-XXL; Pierre et al. 2016). XMM-XXL is a medium-depth X-ray survey that covers a total area of $50\,deg^2$ split into two fields nearly equal in size: the XMM-XXL North (XXL-N) and the XXM-XXL South (XXL-S). The XXL-N dataset consists of 8445 X-ray sources. Of these X-ray sources, 5294 have SDSS counterparts and 2512 have reliable spectroscopy (Menzel et al. 2016; Liu et al. 2016). The mid-IR and near-IR (MIR and NIR) data were obtained following the likelihood ratio method (Sutherland & Saunders 1992) as implemented in (Georgakakis et al. 2011). For more details on the reduction of the XMM observations and the IR identifications of the X-ray sources, we refer to Georgakakis et al. (2017).

2.2. The VIPERS catalogue

The galaxy control sample used in our analysis comes from the public data release 2 (PDR-2; Scodeggio et al. 2018) of the VIPERS survey (Guzzo et al. 2014; Garilli et al. 2014), which partially overlaps with the XMM-XXL field. The observations were carried out using the VIMOS (VIsible MultiObject Spectrograph; Le Fèvre et al. 2003) on the ESO Very Large Telescope (VLT). The survey covers an area of $\approx 23.5\,deg^2$, split over two regions within the Canada-France-Hawaii Telescope Legacy Survey (CFHTLS-Wide) W1 and W4 fields. Follow-up spectroscopic targets were selected to the magnitude limit $i' = 22.5$ from the T0006 data release of the CFHTLS catalogues. An optical colour–colour pre-selection, namely, $[(r-i) > 0.5(u-g)$ or $(r-i) > 0.7]$, excludes galaxies at $z < 0.5$, yielding a >98% completeness for $z > 0.5$ and up to $z \sim 1.2$ (for more details see Guzzo et al. 2014). Then, PDR-2 consists of 86 775 galaxies with available spectra. Each spectrum is assigned a quality flag that quantifies the redshift reliability. In all the VIPERS papers, redshifts with flags in the range between 2 and 9 have been considered to be reliable and are those used in the science analysis (Garilli et al. 2014; Scodeggio et al. 2018). The above criteria yield 45 180 galaxies within the redshift range spanned by the VIPERS survey ($0.5 < z < 1.2$). This is the same galaxy sample used in Mountrichas et al. (2019, see their Sect. 2.1).

To add the NIR and MIR photometry, we cross-matched the VIPERS catalogue with sources in the VISTA Hemisphere Survey (VHS; McMahon et al. 2013) and the AllWISE catalogue from the WISE survey (Wright et al. 2010). The process is described in detail in Sect. 2.5 in Pouliasis et al. (2020). Specifically, the xmatch tool from the astromatch[1] package was used. xmatch utilizes different statistical methods for cross-matching of astronomical catalogues. This tool matches a set of catalogues and gives the Bayesian probabilities of the associations or non-association (Pineau et al. 2017). We only kept sources with a high probability of association (>68%). When one source was associated with several counterparts, we selected the association with the highest probability. 14 128 galaxies from the VIPERS catalogue have counterparts in the NIR and MIR.

3. Galaxy and supermassive black hole properties

In the following, we describe how we obtained measurements for the properties of the sources used in our analysis. Specifically, we present how we measured the SFR and M_* of AGN and non-AGN galaxies, how we calculated the bolometric luminosity (L_{bol}), n_{Edd} and λ_{sBHAR}) of AGN, and how the available M_{BH} were estimated.

3.1. Calculation of SFR and M_*

For the calculation of the SFR and M_* of AGN host galaxies and non-AGN systems, we applied spectral energy distribution (SED) fitting, using the CIGALE algorithm (Boquien et al. 2019; Yang et al. 2020, 2022). CIGALE allows for the inclusion of the X-ray flux in the fitting process and has the ability to account for the extinction of the UV and optical emission in the poles of AGN (Yang et al. 2020; Mountrichas et al. 2021a,b; Buat et al. 2021).

For consistency with our previous studies (Mountrichas et al. 2021c, 2022a,b; Mountrichas & Shankar 2023), we used the same templates and parametric grid in the SED fitting process as those used in these previous works. In brief, the galaxy component is modelled using a delayed SFH model with a function form $SFR \propto t \times \exp(-t/\tau)$. A star formation burst is included (Małek et al. 2018; Buat et al. 2019) as a constant ongoing period of star formation of 50 Myr. Stellar emission was modelled using the single stellar population

[1] https://github.com/ruizca/astromatch

templates of Bruzual & Charlot (2003) and attenuated following the Charlot & Fall (2000) attenuation law. To model the nebular emission, CIGALE adopts the nebular templates based on Villa-Velez et al. (2021). The emission of the dust heated by stars is modelled based on Dale et al. (2014), without any AGN contribution. The AGN emission is included using the SKIRTOR models of Stalevski et al. (2012, 2016). The parameter space used in the SED fitting process is shown in Tables 1 in Mountrichas et al. (2021b, 2022a,b).

CIGALE has the ability to model the X-ray emission of galaxies. In the SED fitting process, the intrinsic L_X in the 2−10 keV band were used. The calculation of the intrinsic L_X is described in detail in Sect. 3.1 in Mountrichas et al. (2021b). In brief, we used the number of photons in the soft (0.5−2 keV) and the hard (2−8 keV) bands that are provided in the Liu et al. (2016) catalogue. Afterwards, a Bayesian approach (BEHR; Park et al. 2006) was applied to calculate the hardness ratio, HR = $\frac{H-S}{H+S}$, of each source, where H and S are the counts in the soft and hard bands, respectively. These hardness ratio measurements are then inserted in the Portable, Interactive, Multi-Mission Simulator tool (PIMMS; Mukai 1993) to estimate the hydrogen column density, N_H, for each source. A power law with slope $\Gamma = 1.8$ for the X-ray spectra was assumed. We note that the value of the galactic N_H is $N_H = 10^{20.25}$ cm^{-1}.

The reliability of the SFR measurements, both in the cases of AGN and non-AGN systems, has been examined in detail in our previous works (as well as e.g., in Sect. 3.2.2 in Mountrichas et al. 2022b). Finally, we note that the AGN module was used when we fit the SEDs of non-AGN systems. This allowed us to uncover AGN that had remained undetected by X-rays (e.g., Pouliasis et al. 2020) and exclude them from our galaxy control sample (see Sect. 4).

3.2. Calculation of SFR_{norm}

The goal of this study is to compare the SFR of AGN host galaxies with the SFR of non-AGN systems as a function of various black hole properties. For the comparison of the SFR of AGN and non-AGN galaxies, we used the SFR_{norm} parameter. SFR_{norm} is measured following the process of our previous studies (e.g., Mountrichas et al. 2021c, 2022a,b). Specifically, the SFR of each X-ray AGN is divided by the SFR of galaxies in the control sample that are within ±0.2 dex in M_* and $\pm 0.075 \times (1+z)$ in redshift. Furthermore, each source is weighted based on the uncertainty of the SFR and M_* measurements made by CIGALE. Then, the median values of these ratios are used as the SFR_{norm} of each X-ray AGN. We note that our measurements are not sensitive to the choice of the box size around the AGN. Selecting smaller boxes, though, has an effect on the errors of the calculations (Mountrichas et al. 2021c). The calculation of SFR_{norm} requires both datasets to be mass complete in the redshift range of interest. This requirement is met in the stellar mass range we perform our analysis (see Sect. 4).

3.3. Black hole mass measurements

Out of the 2512 AGN in the XXL-N catalogue that have reliable spectroscopy from SDSS-III/BOSS (Sect 2), 1786 have been classified as broad line AGN (BLAGN1), by Menzel et al. (2016). One source was classified as BLAGN1 using the full width at half maximum (FWHM) threshold of 1000 km s^{-1}. Liu et al. (2016) performed spectral fits to the BOSS spectroscopy of these 1786 BLAGN1 to estimate single-epoch virial M_{BH} from continuum luminosities and broad line widths (e.g., Shen et al. 2013). The details of the spectral fitting procedure are given in Sect. 3.3 of Liu et al. (2016) and in Shen et al. (2013). In brief, they first measured the continuum luminosities and broad-line FWHMs. Then, they used several single-epoch virial mass estimators to calculate M_{BH}. Specifically, they applied the following fiducial mass recipes, depending on the redshift of the source: Hβ at $z < 0.9$, Mg II at $0.9 < z < 2.2$ and C IV at $z > 2.2$.

Previous studies have shown that single-epoch M_{BH} estimates that use different emission lines, when adopting the fiducial single-epoch mass formula, are generally consistent with each other with negligible systematic offsets and scatter (e.g., Shen et al. 2008, 2011, 2013; Shen & Liu 2012). Liu et al. (2016) confirmed these previous findings. Finally, their M_{BH} measurements have, on average, errors of ∼0.5 dex, whereas sources with a higher signal-to-noise ratio (S/N) have uncertainties of the measured M_{BH} that are less than 0.15 dex.

3.4. Calculating the bolometric luminosity of the AGN, Eddington ratio, and specific black hole accretion rate

There are two measurements available for the L_{bol} of the AGN in our sample. The catalogue of Liu et al. (2016) includes L_{bol} calculations. These have been derived by integrating the radiation directly produced by the accretion process, that is the thermal emission from the accretion disc and the hard X-ray radiation produced by inverse-Compton scattering of the soft disc photons by a hot corona (for more details see their Sect. 4.2). CIGALE also provides L_{bol} measurements. Mountrichas (2023) compared the two L_{bol} estimates and found that their distributions have a mean difference of 0.08 dex with a standard deviation of 0.42 dex. Following Mountrichas (2023), we choose to use the L_{bol} calculations of CIGALE. However, we note that using the L_{bol} measurements from the Liu et al. (2016) catalogue does not affect our results or conclusions.

The n_{Edd} is defined as the ratio of the bolometric luminosity, L_{bol}, and the Eddington luminosity, L_{Edd}. The L_{Edd} measurement is the maximum luminosity that can emitted by the AGN and is determined by the balance between the radiation pressure and the gravitational force exerted by the black hole ($L_{Edd} = 1.26 \times 10^{38}\, M_{BH}/M_\odot$ erg s^{-1}). In our analysis, we used n_{Edd} measurements derived using the L_{bol} calculations from CIGALE, as opposed to those available in the Liu et al. (2016) catalogue. Nevertheless, this choice does not affect our results.

The λ_{sBHAR} is the rate of the accretion onto the SMBH relative to the M_* of the host galaxy. It is often used as a proxy of the Eddington ratio, in particular when black hole measurements are not available. For the calculation of λ_{sBHAR}, the following expression is used:

$$\lambda_{sBHAR} = \frac{k_{bol}\, L_{X,2-10\,keV}}{1.26 \times 10^{38}\ \mathrm{erg\ s^{-1}} \times 0.002 \frac{M_*}{M_\odot}}, \quad (1)$$

where k_{bol} is a bolometric correction factor, which converts the 2−10 keV X-ray luminosity to AGN bolometric luminosity. For our sample, L_{bol} measurements are already available, as described earlier in this section, and thus a bolometric correction is not required. Nevertheless, we chose to use Eq. (1) for the calculation of λ_{sBHAR}, as it is the most common method used to calculate λ_{sBHAR} and it also facilitates a direct comparison with the $SFR_{norm}-\lambda_{sBHAR}$ measurements of our previous studies (Mountrichas et al. 2021c, 2022b). For the same reasons, instead of the M_{BH} measurements that are available for our sources, we chose to use the redshift-independent scaling relation between M_{BH} and bulge mass, M_{bulge}, of Marconi & Hunt (2003),

with the assumption that the $M_{\rm bulge}$ can be approximated by the M_*. Specifically, we used $M_{\rm BH} = 0.002\, M_{\rm bulge}$. Finally, for $k_{\rm bol}$, we adopt the value of $k_{\rm bol} = 25$. This value is used in many studies (e.g., Elvis et al. 1994; Georgakakis et al. 2017; Aird et al. 2018; Mountrichas et al. 2021c, 2022b). Lower values have also be used (e.g., $k_{\rm bol} = 22.4$ in Yang et al. 2017), as well as luminosity-dependent bolometric corrections (e.g., Hopkins et al. 2007; Lusso et al. 2012). In Sect. 5.3.3, we examine how good these approximations are and their impact on the calculation of $\lambda_{\rm sBHAR}$.

4. Final samples

In this section, we describe the criteria we apply to compile the final dataset of X-ray sources, drawn from the XMM-XXL catalogue (Sect. 2.1), and the final control sample of non-AGN galaxies, drawn from the VIPERS survey (Sect. 2.2).

4.1. The final X-ray dataset

We needed to use only sources (X-ray and non-AGN galaxies) that have the most reliable M_* and SFR measurements. For that purpose, for the X-ray sources, we used the final sample presented in Mountrichas (2023). A detailed description of the photometric and reliability criteria that were applied is provided in Sect. 2.4 of that study. In brief, we require our sources to have measurements in the following photometric bands: u, g, r, i, z, J, H, K, $W1$, $W2$, and $W4$, where $W1$, $W2$, and $W4$ are the WISE photometric bands at 3.4, 4.6 and 22 µm. To exclude sources with bad SED fits and unreliable host galaxy measurements, a reduced χ^2 threshold of $\chi^2_r < 5$ was imposed (e.g., Masoura et al. 2018; Buat et al. 2021). We also excluded systems for which CIGALE could not constrain the parameters of interest (SFR, M_*). To this end, the two values that CIGALE provides for each estimated galaxy property are used. One value corresponds to the best model and the other (Bayesian) value is the likelihood-weighted mean value. A large difference between the two calculations suggests a complex likelihood distribution and important uncertainties. We therefore only include in our analysis sources with $\frac{1}{5} \leq \frac{\rm SFR_{best}}{\rm SFR_{bayes}} \leq 5$ and $\frac{1}{5} \leq \frac{M_{*,\rm best}}{M_{*,\rm bayes}} \leq 5$, where $\rm SFR_{best}$ and $M_{*,\rm best}$ are the best-fit values of SFR and M_*, respectively and $\rm SFR_{bayes}$ and $M_{*,\rm bayes}$ are the Bayesian values estimated by CIGALE. 687 broad-line, X-ray AGN with spectroscopic redshifts meet the above requirements and also have available $M_{\rm BH}$ measurements in the catalogue of Liu et al. (2016).

We then restricted the redshift range of the X-ray dataset to match that of the galaxy control sample (i.e., the VIPERS survey, $0.5 \leq z \leq 1.2$). Altogether, 240 AGN meet this requirement. In Mountrichas et al. (2021c, 2022a,b), we found that the $\rm SFR_{norm}$−$L_{\rm X}$ relation depends on the M_* range probed by the sources. Specifically a flat $\rm SFR_{norm}$−$L_{\rm X}$ relation was found for the least and most massive systems ($\log[M_*(M_\odot)] < 10.5$ and $\log[M_*(M_\odot)] > 11.5$), with $\rm SFR_{norm} \sim 1$. However, for intermediate stellar masses ($10.5 < \log[M_*(M_\odot)] < 11.5$), the value of $\rm SFR_{norm}$ was found to be ≤1 at low-to-moderate $L_{\rm X}$ ($\log[L_{\rm X,2-10\,keV}(\rm erg\,s^{-1})] < 44$); whereas at higher $L_{\rm X}$, $\rm SFR_{norm} > 1$ (e.g., see Fig. 5 in Mountrichas et al. 2022a). Therefore, in this study, we restricted the analysis to those sources with $10.5 < \log[M_*(M_\odot)] < 11.5$. Within this M_* range, both of our datasets are also mass-complete (Davidzon et al. 2013; Mountrichas & Shankar 2023), as required for the calculation of $\rm SFR_{norm}$.

Following previous studies that examined the impact of the AGN feedback on their host galaxies, by calculating $\rm SFR_{norm}$ using only star-forming systems (e.g., Mullaney et al. 2015; Masoura et al. 2018; Mountrichas et al. 2021c), we exclude quiescent (Q) systems from our sources. To identify Q galaxies, we used the distribution of the specific SFR $\left(\rm sSFR = \frac{SFR}{M_*}\right)$ measurements of the galaxy control sample (e.g., similarly to Mountrichas et al. 2021c, 2022a,b). Mountrichas & Shankar (2023), applied this methodology on sources in the XMM-XXL field to classify galaxies as Q. From their subset of Q sources, 19 are among our 178 AGN. Their exclusion results in 159 X-ray systems. We note that the inclusion of the 19 AGN hosted by Q systems in our analysis does not affect our overall results and conclusions.

Since the galaxy control sample used in this study is smaller compared to those used in our previous works (see next section), we applied a final criterion to ensure that the $\rm SFR_{norm}$ calculations of each AGN that is included in our analysis are robust. That is to say, we only used AGN whose $\rm SFR_{norm}$ was calculated by matching the X-ray sources with at least 300 sources in the galaxy control sample. Increasing this threshold reduces significantly the size of the X-ray dataset; while at lower values, the scatter of our measurements is higher. A total of 122 X-ray AGN fulfill all the aforementioned criteria. Their $L_{\rm X}$ and $M_{\rm BH}$ values as a function of redshift are presented in Fig. 1.

4.2. The final galaxy control sample

For the galaxy control sample, we apply the same photometric selection criteria and reliability requirements that we applied for the X-ray AGN sample. In addition, we excluded some sources that are included in the X-ray catalogue and we identified and rejected non-X-ray AGN systems. Specifically, we used the CIGALE measurements and excluded sources with $\rm frac_{AGN} > 0.2$, consistently with our previous studies (Mountrichas et al. 2021c, 2022a,b). Here, $\rm frac_{AGN}$ is the fraction of the total IR emission coming from the AGN. This excludes ∼60% of the sources in the galaxy reference catalogue. This fraction is in line with our previous studies. A detailed analysis of the $\rm frac_{AGN}$ criterion is provided in Sect. 3.3 in Mountrichas et al. (2022a). A total of 3622 galaxies fulfill all the aforementioned requirements. Finally, we excluded quiescent galaxies following the process described in the previous section. There are 3371 galaxies that remain and these are the sources in our control sample that we include in the analysis.

5. Results and discussion

In this section, we compare the SFR of AGN and non-AGN galaxies as a function of various black hole properties. Specifically, we study $\rm SFR_{norm}$ as a function of $L_{\rm X}$, $M_{\rm BH}$, $n_{\rm Edd}$, and $\lambda_{\rm sBHAR}$. In Fig. 2, we present the four SMBH properties for the final X-ray dataset. We also apply three correlation statistics: one parametric (Pearson) and two non-parametric statistics (Spearman and Kendall) to quantify the correlations among them. The p-values are presented in Table 1. All parameters are strongly correlated with each other with the exception of the $n_{\rm edd}$−$L_{\rm X}$.

5.1. $\rm SFR_{norm}$ as a function of X-ray luminosity

First, we examined $\rm SFR_{norm}$ as a function of $L_{\rm X}$. The results are shown in the top-left panel of Fig. 3. The small, blue circles present the measurements for individual AGN, while the large,

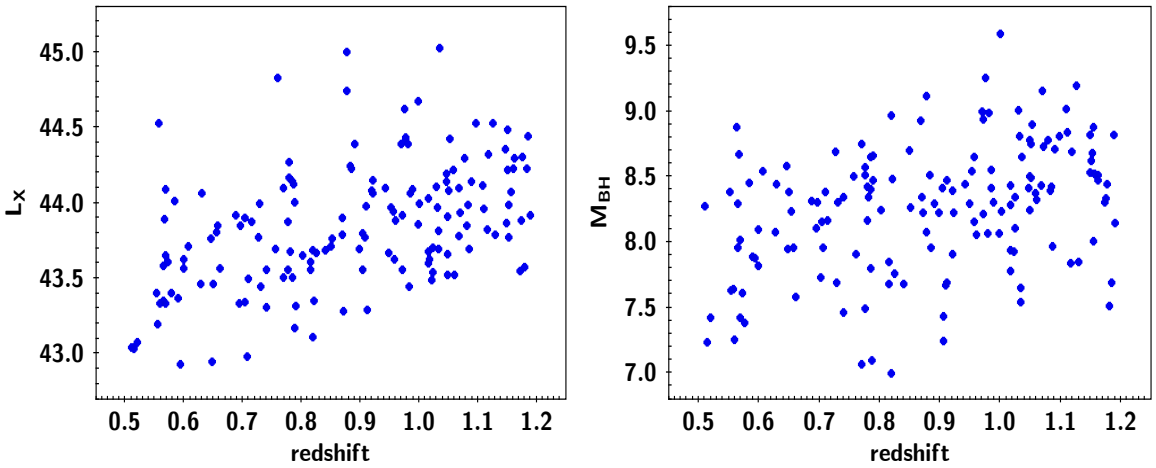

Fig. 1. L_X (left panel) and M_{BH} (right panel) as a function of redshift, for the 122 X-ray AGN used in our analysis.

red circles show the binned results. For the latter, the measurements are grouped in bins of L_X of size 0.5 dex. The errors presented are 1σ errors, calculated via bootstrap resampling (e.g., Loh 2008). We find that the SFR of AGN is lower or at most equal to that of non-AGN galaxies ($SFR_{norm} \leq 1$) at low and moderate L_X ($\log[L_{X,2-10\,keV}(erg\,s^{-1})] \leq 44$) increases at higher L_X, in agreement with previous studies (Mountrichas et al. 2021c, 2022a,b).

The p-values from the three correlation statistics we use to calculate the correlation between SFR_{norm} and L_X are presented in Table 2. The results indicate a strong correlation between the two parameters, independent of the statistical method applied.

5.2. SFR_{norm} as a function of black hole mass

In a recent study, Piotrowska et al. (2022), analyzed three cosmological hydrodynamical simulations (Eagle, Illustris, and IllustrisTNG), by utilizing a random forest classification. They searched for the most effective parameter to separate star-forming and quenched galaxies in the Local Universe. They considered stellar mass, dark matter halo mass, black hole accretion rate, and black hole mass in their investigation. Their analysis showed that black hole mass was the most predictive parameter of galaxy quenching. Bluck et al. (2023), extended these results from the Local Universe to cosmic noon. These findings suggest that the cumulative impact of AGN feedback on a galaxy is encapsulated in the mass of the supermassive black hole and not in the X-ray luminosity, which is a proxy of the current accretion rate.

Hence, we chose to examine the SFR_{norm} as a function of black hole mass. Our goal is to examine if SFR_{norm} and M_{BH} are correlated and compare their correlation with that between SFR_{norm} and L_X. The top-right panel of Fig. 3 presents the SFR_{norm} as a function of M_{BH}. The results show that SFR_{norm} increases with M_{BH} on the full range of black hole masses spanned by our dataset. Specifically, in galaxies that host AGN with low M_{BH} ($\log[M_{BH}(M_\odot)] < 8$), their SFR is lower or equal to the SFR of non-AGN systems. Then, AGN with more massive black holes ($\log[M_{BH}(M_\odot)] > 8.5$) reside in galaxies that cause their SFRs to be enhanced compared to non-AGN. The correlation analysis (Table 2) suggests a strong correlation between SFR_{norm} and M_{BH}.

We also split our datasets into two redshift bins, using a threshold at $z = 0.9$ and repeat the correlation analysis. The choice of the redshift cut is twofold. Primarily, it aligns with the median redshift of the AGN sample. Furthermore, this redshift value corresponds to the redshift at which different spectral lines have been used for the calculation of M_{BH} (see Sect. 3.3). The results are presented in Tables 3 and 4. The same trends are observed with those using sources in the full redshift interval, that is a strong correlation is found between SFR_{norm} and M_{BH} in both redshift ranges. However, this correlation appears less strong in the lowest redshift interval compared to that found in the highest redshift bin. This could imply that the correlation between the two properties is, mainly, driven by massive M_{BH} ($M_{BH} \gtrsim 10^{8.5}\,M_\odot$) that are poorly detected at $z < 0.9$ in the dataset used in our analysis (Fig. 1). This interpretation is also supported by the strong correlation between L_X and M_{BH} (Fig. 2) combined with the results from previous studies that have shown that the $SFR_{norm}-L_X$ relation is nearly flat at $L_X < 10^{44}\,erg\,s^{-1}$ and shows a positive correlation only at higher L_X (Mountrichas et al. 2021c, 2022a,b).

A comparison of the p-values with those in the previous section, shows that the correlation between SFR_{norm} and M_{BH} is similar to that between SFR_{norm} and L_X. Subsequently, we explore whether this observation holds when considering the associated uncertainties of L_X and M_{BH}. For that purpose, we utilize the linmix module (Kelly 2007) that performs linear regression between two parameters, by repeatedly perturbing the datapoints within their uncertainties. The p-values obtained are 3.2×10^{-5} and 7.6×10^{-4} for the $SFR_{norm}-L_X$ and $SFR_{norm}-M_{BH}$, respectively. These findings suggest, that despite accounting for uncertainties in L_X and M_{BH} measurements, there exists a robust correlation between these two properties and SFR_{norm} and that the two correlations are indeed similar.

As shown in Fig. 2 and Table 1, L_X and M_{BH} are strongly correlated. To investigate further the correlation among SFR_{norm}, L_X and M_{BH}, we perform a partial-correlation analysis (PCOR). PCOR measures the correlation between two variables while controlling for the effects of a third (e.g., Lanzuisi et al. 2017; Yang et al. 2017; Mountrichas et al. 2022b). We use one parametric statistic (Pearson) and one non-parametric statistic (Spearman). Table 5 lists the results of the p-values. Regardless of the parametric statistic of choice, p-values for the $SFR_{norm}-M_{BH}$ relation are smaller compared to the corresponding p-values for the $SFR_{norm}-L_X$ relation. This implies that the correlation between SFR_{norm} and M_{BH} is more robust compared to that with L_X, even when factoring in the existing correlation

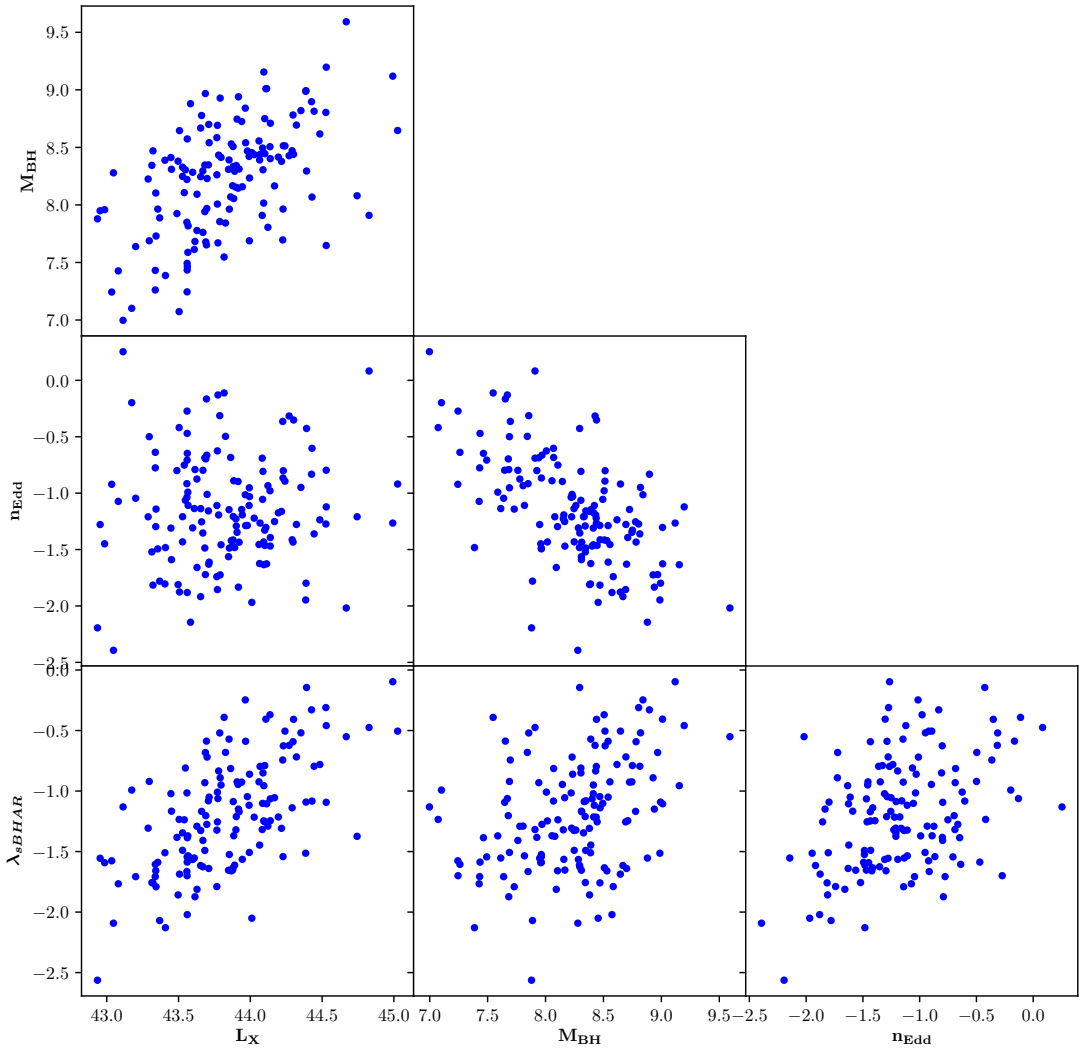

Fig. 2. Correlations among the four SMBH properties used in our study. Specifically, we present the correlations among the $M_{\rm BH}$, the $L_{\rm X}$, the specific black hole accretion rate $\left(\lambda_{\rm sBHAR} \propto \frac{L_{\rm X}}{M_*}\right)$, and the Eddington ratio $\left(n_{\rm Edd} \propto \frac{L_{\rm bol}}{M_{\rm BH}}\right)$. The p-values from the correlation analysis are shown in Table 1.

Table 1. p-values from the correlation analysis we apply for the four SMBH properties used in our analysis.

Relation	Pearson	Spearman	Kendall
$M_{BH}-L_{\rm X}$	2.1×10^{-11}	3.4×10^{-11}	6.5×10^{-11}
$n_{\rm Edd}-L_{\rm X}$	0.40	0.59	0.51
$\lambda_{\rm sBHAR}-L_{\rm X}$	2.9×10^{-15}	2.0×10^{-14}	2.6×10^{-13}
$n_{\rm Edd}-M_{\rm BH}$	4.7×10^{-15}	6.5×10^{-14}	1.1×10^{-12}
$\lambda_{\rm sBHAR}-M_{\rm BH}$	6.6×10^{-6}	6.7×10^{-6}	5.2×10^{-6}
$\lambda_{\rm sBHAR}-n_{\rm Edd}$	6.1×10^{-7}	1.4×10^{-5}	1.3×10^{-5}

between $M_{\rm BH}$ and $L_{\rm X}$. This deduction remains valid even when we partition the dataset into two redshift bins, specifically at $z = 0.9$.

Mountrichas et al. (2022b) applied PCOR analysis on sources in the COSMOS field and found that $\rm SFR_{norm}$ is correlated stronger with M_* than with $L_{\rm X}$. Yang et al. (2017) used galaxies in the CANDELS/GOODS-South field and examined the correlation between the black hole accretion rate (BHAR; which is measured directly from the $L_{\rm X}$), SFR and M_*. They found that the BHAR is linked mainly to M_* rather than SFR. There is also a well known correlation between the M_* and the $M_{\rm BH}$ (e.g., Merloni et al. 2010; Sun et al. 2015; Suh et al. 2020; Setoguchi et al. 2021; Poitevineau et al. 2023). Recently, Mountrichas (2023) reported such a correlation between $M_{\rm BH}$ and M_* using AGN in the XMM-XXL field, which is the same X-ray dataset used in this work. We applied a PCOR analysis, this time among $\rm SFR_{norm}$, $M_{\rm BH}$, and M_*. The results (presented in Table 6, top two lines) suggest that $\rm SFR_{norm}$ is linked more to $M_{\rm BH}$ than M_*. However, we note that for the reasons mentioned in Sect. 4, our datasets have been restricted to a relatively narrow M_* range ($10.5 < \log[M_*(M_\odot)] < 11.5$). Therefore, although the $M_{\rm BH}$ parameter spans ~2.5 orders of magnitude, that of M_* spans only an order of magnitude among our samples.

To increase the M_* range that our sources could probe, we lifted the M_* requirement. There are 209 AGN and 4454 galaxies within $10 < \log[M_*(M_\odot)] < 12$. Using these two subsets, we calculated the $\rm SFR_{norm}$ for the 240 AGN and then we applied a PCOR analysis among $\rm SFR_{norm}$, $M_{\rm BH}$ and M_*. The results are presented in the two bottom lines of Table 6. The p-values of the non-parametric statistic (Spearman) are similar;

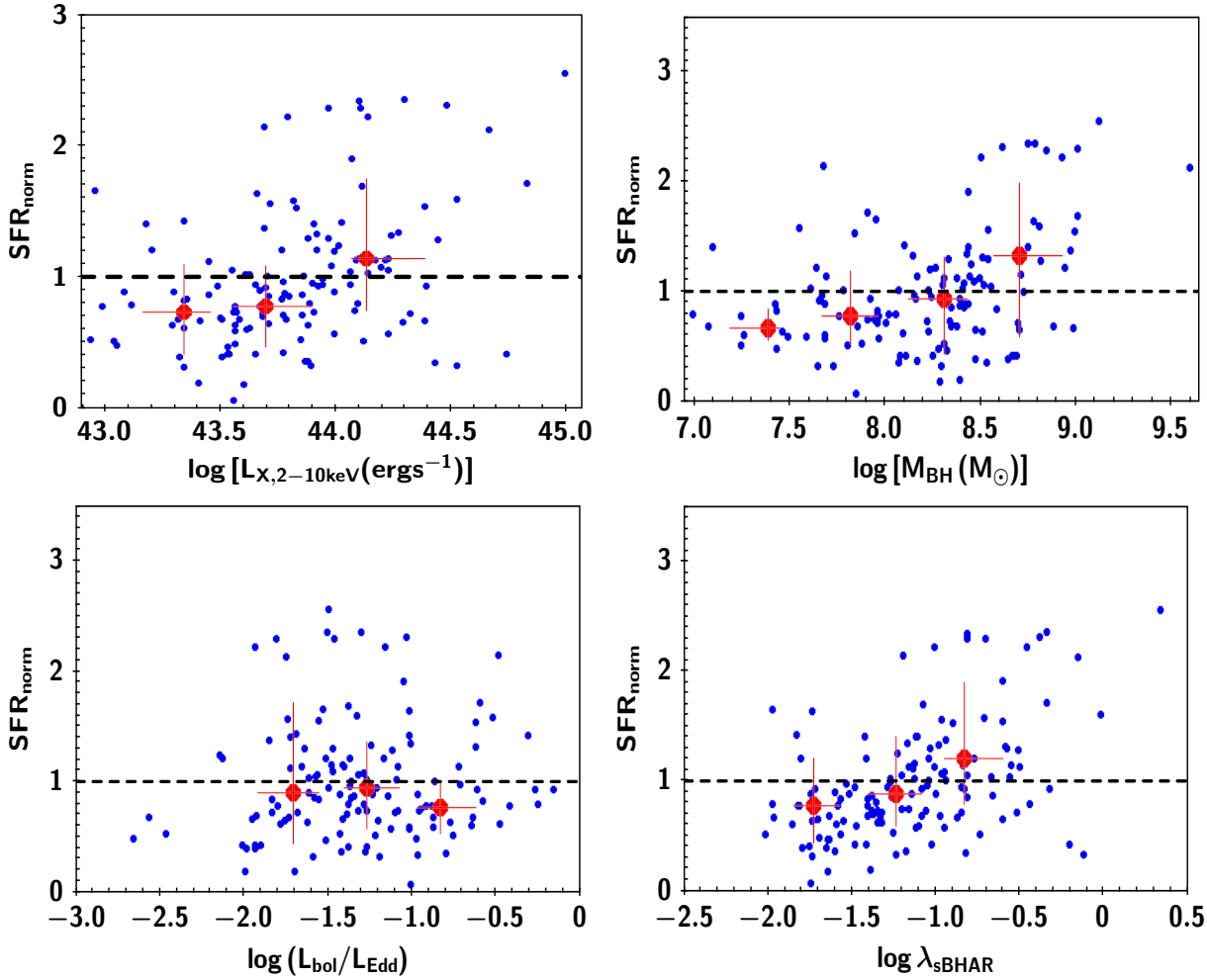

Fig. 3. SFR_{norm} as a function of SMBH properties. The SFR_{norm} parameter as a function of L_X (top, left panel), M_{BH} (top, right panel), Eddington ratio (bottom, left panel), and λ_{sBHAR} (bottom, right panel) are presented.

Table 2. *p*-values of correlation analysis, using sources with $0.5 \leq z \leq 1.2$.

Relation	Pearson	Spearman	Kendall
$SFR_{norm}-L_X$	3.1×10^{-6}	2.9×10^{-7}	1.4×10^{-7}
$SFR_{norm}-M_{BH}$	4.0×10^{-7}	3.3×10^{-7}	2.9×10^{-7}
$SFR_{norm}-n_{Edd}$	0.87	0.56	0.58
$SFR_{norm}-\lambda_{sBHAR}$	6.3×10^{-5}	5.1×10^{-6}	3.0×10^{-6}

Table 3. *p*-values of correlation analysis, using sources with $0.5 \leq z \leq 0.9$.

Relation	Pearson	Spearman	Kendall
$SFR_{norm}-L_X$	8.0×10^{-3}	5.0×10^{-3}	4.1×10^{-3}
$SFR_{norm}-M_{BH}$	2.1×10^{-3}	4.2×10^{-3}	4.4×10^{-3}
$SFR_{norm}-n_{Edd}$	0.75	0.48	0.48
$SFR_{norm}-\lambda_{sBHAR}$	7.0×10^{-2}	9.1×10^{-3}	1.2×10^{-2}

however, the *p*-value using the parametric statistic (Pearson) are lower for the $SFR_{norm}-M_{BH}$, suggesting that the correlation between $SFR_{norm}-M_{BH}$ is stronger than the correlation between $SFR_{norm}-M_*$. We note that these results should be taken with caution since our samples are not mass-complete in the full M_* range that is considered in this exercise – and specifically within $10.0 < \log[M_*(M_\odot)] < 10.5$.

Overall, we conclude that SFR_{norm} is mostly linked to M_{BH} rather than L_X. Our results also suggest that the $SFR_{norm}-M_*$ correlation is due to the underlying M_*-M_{BH}. The picture that emerges corroborates the idea that the M_{BH} is a more robust tracer of AGN feedback compared to the instantaneous activity of the SMBH – represented by L_X – and as such M_{BH} is a better predictive parameter of the changes of the SFR of the host galaxy, as theoretical studies have also suggested (Piotrowska et al. 2022; Bluck et al. 2023). Our results are also in line with the aforementioned studies regarding the negative AGN feedback they report, at least up to $M_{BH} \sim 10^{8.5}\,M_\odot$ (i.e., $SFR_{norm} < 1$). The increase in SFR_{norm} that we detect in our results suggests that this negative feedback may become less impactful on the SFR of the host galaxy, as we transition to systems with more massive SMBHs. These studies have additionally shown that the fraction of quenched galaxies increases with M_{BH}. To investigate this claim, we would need to examine the fraction of quiescent systems as a function of M_{BH} in our dataset. However, the small sample size used in our analysis and the low number of quiescent systems included do not allow for such an investigation.

Table 4. p-values of correlation analysis, using sources with $0.9 < z \leq 1.2$.

Relation	Pearson	Spearman	Kendall
$SFR_{norm}-L_X$	6.9×10^{-7}	4.6×10^{-7}	1.1×10^{-6}
$SFR_{norm}-M_{BH}$	1.7×10^{-7}	2.6×10^{-7}	1.7×10^{-6}
$SFR_{norm}-n_{Edd}$	0.82	0.32	0.31
$SFR_{norm}-\lambda_{sBHAR}$	1.4×10^{-6}	8.4×10^{-7}	2.8×10^{-6}

Table 5. p-values of partial correlation analysis, among SFR_{norm}, L_X and M_{BH}.

	Pearson	Spearman
$SFR_{norm}-L_X$	0.056	0.016
$SFR_{norm}-M_{BH}$	7×10^{-5}	9×10^{-5}

5.3. SFR_{norm} as a function of Eddington ratio and specific black hole accretion rate

In this section, we investigate the correlation between SFR_{norm} and two other SMBH properties that represent the instantaneous AGN activity. Specifically, we study the relation between $SFR_{norm}-n_{Edd}$ and $SFR_{norm}-\lambda_{sBHAR}$. We also examine whether λ_{sBHAR} is a good proxy of the n_{Edd}.

5.3.1. SFR_{norm} as a function of Eddington ratio

The Eddington ratio provides another important property of the SMBH. Setoguchi et al. (2021) used 85 moderately luminous ($\log L_{bol} \sim 44.5$–$46.5\,erg\,s^{-1}$) AGN from the Subaru/*XMM-Newton* Deep Field (SXDF) and found a strong correlation between the SFR of AGN and n_{Edd} (correlation coefficient: $r = 0.62$). Recently, Georgantopoulos et al. (2023) studied the stellar populations of obscured and unobscured AGN at $0.6 < z < 1.0$. Based on their analysis, the stellar age of both AGN types increases at lower Eddington ratio values (see the bottom-left panel of their Fig. 4 and top-right panel of their Fig. 11).

The bottom, left panel of Fig. 3, presents our calculations for SFR_{norm} as a function of the Eddington ratio. The value of SFR_{norm} remains roughly constant regardless of the value of n_{Edd}. This is confirmed by the results of the correlation analysis, shown in Table 2 (see also Tables 3 and 4 for different redshift intervals). This nearly flat $SFR_{norm}-n_{Edd}$ relation can be explained by the correlations among the M_{BH}, L_X and n_{Edd}, presented in Fig. 2. There is a strong anti-correlation between n_{Edd} and M_{BH}, but a positive correlation between n_{Edd} and L_X, while a strong positive correlation is detected between M_{BH} and L_X. We note that when we examine the relation between the SFR of AGN and n_{Edd}, we find a (strong) correlation ($r = 0.54$), similar to that found by Setoguchi et al. (2021).

5.3.2. SFR_{norm} as a function of the specific black hole accretion rate

The specific black hole accretion rate is often used as a proxy of the Eddington ratio. Previous studies found an increase in the SFR_{norm} with λ_{sBHAR} (see Figs. 10 and 11 in Mountrichas et al. 2021c, 2022b, respectively). Pouliasis et al. (2022) used X-ray AGN in the COSMOS, XMM-XXL and eFEDS, at $z > 3.5$ and found that AGN that lie inside or above the main sequence (i.e., $SFR_{norm} \geq 1$) exhibit higher λ_{sBHAR} values compared to X-ray sources that lie below the MS.

Our results, presented in the bottom- right panel of Fig. 3, agree with these previous findings. Specifically, we observe an increase in SFR_{norm} with λ_{sBHAR}. The application of a correlation analysis shows that there is a strong correlation between the two parameters, albeit not as strong as the correlation found between $SFR_{norm}-L_X$ and $SFR_{norm}-M_{BH}$ (Tables 2–4).

Mountrichas et al. (2022b) examined the correlation between SFR_{norm} and λ_{sBHAR} using X-ray sources in the COSMOS field and compared their results with those using AGN in the Boötes, presented in Mountrichas et al. (2021c) (see Fig. 11 and Table 5 in Mountrichas et al. 2022b). Although both datasets present a nearly, linear increase in the SFR_{norm} with L_X, the amplitude of SFR_{norm} differs for the same λ_{sBHAR} values, for the two datasets. They attributed this difference to the different properties of the AGN from the two samples included in λ_{sBHAR} bins of the same value. Specifically, COSMOS sources are less luminous and less massive than their Boötes counterparts in λ_{sBHAR} bins of similar values. Therefore, if a dataset probes AGN within a large range of L_X and M_*, this could increase the scatter of SFR_{norm} for the same λ_{sBHAR} values, thus weakening the correlation between SFR_{norm} and λ_{sBHAR} and rendering λ_{sBHAR} useless as a parameter with respect to studying the impact of AGN feedback on the SFR of the host galaxy.

Table 6. p-values of partial correlation analysis, among SFR_{norm}, M_*, and M_{BH}.

	Pearson	Spearman
$SFR_{norm}-M_*$	0.515	0.0068
$SFR_{norm}-M_{BH}$	1.6×10^{-8}	2.5×10^{-9}
$SFR_{norm}-M_*$ (ext)	0.027	2×10^{-6}
$SFR_{norm}-M_{BH}$ (ext)	1.1×10^{-5}	5×10^{-6}

Notes. The top two lines present the results using sources within $10.5 < \log[M_*(M_\odot)] < 11.5$. The bottom two lines present the results within $10 < \log[M_*(M_\odot)] < 12$.

5.3.3. Considering λ_{sBHAR} as a good proxy for the Eddington ratio

As mentioned in the previous section, λ_{sBHAR} is often used as a proxy of n_{Edd} on the basis that there is a linear relation between the M_* and M_{BH} and that L_{bol} can be inferred by L_X. Prompted by the different relations found between $SFR_{norm}-n_{Edd}$ and $SFR_{norm}-\lambda_{sBHAR}$, we investigated this possibility further.

Lopez et al. (2023) used X-ray selected AGN in the miniJPAS footprint and found (among other aspects) that the Eddington ratio and λ_{sBHAR} have a difference of 0.6 dex. They attributed this difference to the scatter on the $M_{BH}-M_*$ relation of their sources. The median value of n_{Edd} of our sample, calculated using the L_{bol} measurements of CIGALE, is $n_{Edd} = -1.26$, ($n_{Edd} = -1.33$, using the values available in the Liu et al. 2016, catalogue). The median value of λ_{sBHAR}, estimated using Eq. (1), is $\lambda_{sBHAR} = -1.08$. Thus, we find a median difference of $\sim$0.25 between n_{Edd} and λ_{sBHAR}. Although this difference is lower than that reported by Lopez et al. (2023), below we examine the cause of it.

We re-calculated λ_{sBHAR}, using the L_{bol} measurements from CIGALE (see Sect. 3.4) instead of the product of $k_{bol}\,L_X$. In this case, the median value of λ_{sBHAR} is -1.25. This value is in

excellent agreement with that of $n_{\rm Edd}$ (−1.26), using for the calculation of the latter the $L_{\rm bol}$ measurements from CIGALE. We also calculated $\lambda_{\rm sBHAR}$ keeping the same numerator as in Eq. (1), but using the $M_{\rm BH}$ measurements available in our dataset instead of the $M_{\rm BH}$−M_* scaling relation. In this case, the median difference between the distributions of $\lambda_{\rm sBHAR}$ and $n_{\rm Edd}$ is ∼0.08. We note that for the sources used in our analysis, the scaling relation between $M_{\rm BH}$ and M_* is, $M_{\rm BH} \approx 0.003\,M_*$ (see also Sect. 3.3 in Mountrichas 2023), which is in good agreement with the $M_{\rm BH} = 0.002\,M_{\rm bulge}$ used in Eq. (1).

Therefore, the way $L_{\rm bol}$ is calculated seems to play an equally important role with the $M_{\rm BH}$−M_* scaling relation on the comparison between $n_{\rm Edd}$ and $\lambda_{\rm sBHAR}$ in our sample. The mean difference between the $L_{\rm bol}$ calculated by CIGALE and the product of $k_{\rm bol}\,L_{\rm X}$ is 0.24 dex, with a dispersion of 0.35. CIGALE measurements suggest a mean $k_{\rm bol} = 14.8$ (i.e., a mean difference of zero for the two $L_{\rm bol}$ measurements). Finally, we compared the $L_{\rm bol}$ measurements of CIGALE with those using a luminosity dependent $k_{\rm bol}$. Specifically, we used the prescription of Lusso et al. (2012), using the values presented in their Table 2 for their spectroscopic type-1 AGN. In this case, the two calculations are in very good agreement with a mean difference of 0.04 dex and a dispersion of 0.34. Figure 4 presents the comparison between the $L_{\rm bol}$ measurements using the formula presented in Lusso et al. (2012) and CIGALE.

We conclude that caution has to be taken when $\lambda_{\rm sBHAR}$ is used as a proxy of $n_{\rm Edd}$, since the calculation of $L_{\rm bol}$ and the scatter in the $M_{\rm BH}$−M_* scaling relation can cause (large) discrepancies between the estimated values of the two parameters.

6. Conclusions

We used 122 X-ray AGN in the XMM-XXL-N field and 3371 VIPERS galaxies, within the redshift and stellar mass ranges of $0.5 \leq z \leq 1.2$ and $10.5 < \log[M_*(M_\odot)] < 11.5$, respectively. The X-ray sources probe luminosities within $43 < \log[L_{\rm X,2-10\,keV}({\rm ergs}^{-1})] < 45$. Both populations meet strict photometric selection criteria and various selection requirements to ensure that only sources with robust (host) galaxy measurements are included in the analysis. The latter have been calculated via SED fitting, using the CIGALE code. Using these datasets, we calculated the $\rm SFR_{norm}$ parameter to compare the SFR of AGN with the SFR of non-AGN galaxies, as a function of various black hole properties. Specifically, we examined the correlations of $\rm SFR_{norm}$ with the $L_{\rm X}$, $M_{\rm BH}$, $n_{\rm Edd}$ and $\lambda_{\rm sBHAR}$. Our main results can be summarized as follows:

– Those AGNs with low black hole masses ($\log(M_{\rm BH}/M_*) < 8$) have lower or at most equal SFR compared to that of non-AGN galaxies, while AGN with more massive black holes ($\log(\rm M_{BH}/M_*) > 8.5$) tend to live in galaxies with (mildly) enhanced SFR compared to non-AGN systems.
– The $\rm SFR_{norm}$ parameter is strongly correlated with both $L_{\rm X}$ and $M_{\rm BH}$. However, the correlation between $\rm SFR_{norm}$−$M_{\rm BH}$ is stronger compared to the correlation between $\rm SFR_{norm}$−$L_{\rm X}$. Our results also suggest that $M_{\rm BH}$ drives the correlation between $\rm SFR_{norm}$−M_* that has been found in previous studies.
– We do not detect a significant correlation between $\rm SFR_{norm}$ and Eddington ratio.
– A correlation is found between $\rm SFR_{norm}$ and specific black hole accretion rate. However, this correlation is weaker compared to that between $\rm SFR_{norm}$−$L_{\rm X}$ and $\rm SFR_{norm}$−$M_{\rm BH}$ and its scatter may increase for samples that span a wide range of $L_{\rm X}$ and M_*.

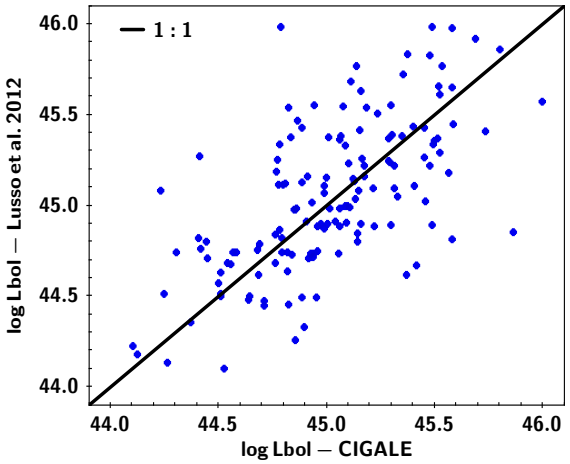

Fig. 4. Comparison of the $L_{\rm bol}$ calculations of CIGALE with the $L_{\rm bol}$ measurements using the formula derived in Lusso et al. (2012). The two measurements are in very good agreement with a mean difference of 0.04 dex. and a dispersion of 0.34.

– The estimation of the AGN bolometric luminosity and the scatter of the $M_{\rm BH}$−M_* scaling relation may cause discrepancies between the specific black hole accretion rate and the Eddington ratio measurements. Therefore, caution has to be taken when the former is used as a proxy for the latter.

These results suggest that there is a strong correlation between $\rm SFR_{norm}$ and AGN activity when the latter is represented by $L_{\rm X}$, $\lambda_{\rm sBHAR}$, and $M_{\rm BH}$. A flat relation was only found between $\rm SFR_{norm}$ and $n_{\rm Edd}$, that can be interpreted as the net result of the different correlations (i.e., positive and negative) among $n_{\rm edd}$, $M_{\rm BH}$, and $L_{\rm X}$ (Fig. 2). Based on our analysis, $M_{\rm BH}$ is the most robust tracer of AGN feedback and the best predictive parameter of the changes of the SFR of the host galaxy.

Acknowledgements. This project has received funding from the European Union's Horizon 2020 research and innovation program under grant agreement no. 101004168, the XMM2ATHENA project. The project has received funding from Excellence Initiative of Aix-Marseille University–AMIDEX, a French 'Investissements d'Avenir' programme. This work was partially funded by the ANID BASAL project FB210003. M.B. acknowledges support from FONDECYT regular grant 1211000. This research has made use of TOPCAT version 4.8 (Taylor 2005).

References

Aird, J., Coil, A. L., & Georgakakis, A. 2018, MNRAS, 474, 1225
Alexander, D. M., & Hickox, R. C. 2012, New Astron. Rev., 56, 93
Bernhard, E., Grimmett, L. P., Mullaney, J. R., et al. 2019, MNRAS, 483, L52
Bluck, A. F. L., Piotrowska, J. M., & Maiolino, R. 2023, ApJ, 944, 108
Boquien, M., Burgarella, D., Roehlly, Y., et al. 2019, A&A, 622, A103
Bower, R. G., Benson, A. J., & Crain, R. A. 2012, MNRAS, 422, 2816
Boyle, B. J., Shanks, T., Croom, S. M., et al. 2000, MNRAS, 317, 1014
Brown, A., Nayyeri, H., Cooray, A., et al. 2019, ApJ, 871, 87
Bruzual, G., & Charlot, S. 2003, MNRAS, 344, 1000
Buat, V., Ciesla, L., Boquien, M., Małek, K., & Burgarella, D. 2019, A&A, 632, A79
Buat, V., Mountrichas, G., Yang, G., et al. 2021, A&A, 654, A93
Charlot, S., & Fall, S. M. 2000, ApJ, 539, 718
Dale, D. A., Helou, G., Magdis, G. E., et al. 2014, ApJ, 784, 83
Davidzon, I., Bolzonella, M., Coupon, J., et al. 2013, A&A, 558, A23
Dubois, Y., Peirani, S., Pichon, C., et al. 2016, MNRAS, 463, 3948
Dunn, R. J. H., & Fabian, A. C. 2006, MNRAS, 373, 959
Elvis, M., Wilkes, B. J., McDowell, J. C., et al. 1994, ApJS, 95, 1
Ferrarese, L., & Merritt, D. 2000, ApJ, 539, 9
Florez, J., Jogee, S., Sherman, S., et al. 2020, MNRAS, 497, 3273

Garilli, B., Guzzo, L., Scodeggio, M., et al. 2014, A&A, 562, A23
Georgakakis, A., Coil, A. L., Willmer, C. N. A., et al. 2011, MNRAS, 418, 2590
Georgakakis, A., Salvato, M., Liu, Z., et al. 2017, MNRAS, 469, 3232
Georgantopoulos, I., Pouliasis, E., Mountrichas, G., et al. 2023, A&A, 673, A67
Guzzo, L., Scodeggio, M., Garilli, B., et al. 2014, A&A, 566, A108
Häring, N., & Rix, H.-W. 2004, ApJ, 604, L89
Hopkins, P. F., Richards, G. T., & Hernquist, L. 2007, ApJ, 654, 731
Jahnke, K., Bongiorno, A., Brusa, M., et al. 2009, ApJ, 706, 215
Kelly, B. C. 2007, ApJ, 665, 1489
Komatsu, E., Smith, K. M., Dunkley, J., et al. 2011, ApJS, 192, 18
Koutoulidis, L., Mountrichas, G., Georgantopoulos, I., Pouliasis, E., & Plionis, M. 2022, A&A, 658, A35
Lanzuisi, G., Delvecchio, I., Berta, S., et al. 2017, A&A, 602, A13
Le Fèvre, O., Saisse, M., Mancini, D., et al. 2003, in Instrument Design and Performance for Optical/Infrared Ground-based Telescopes, eds. M. Iye, & A. F. M. Moorwood, SPIE Conf. Ser., 4841, 1670
Liu, Z., Merloni, A., Georgakakis, A., et al. 2016, MNRAS, 459, 1602
Loh, J. M. 2008, ApJ, 681, 726
Lopez, I. E., Brusa, M., Bonoli, S., et al. 2023, A&A, 672, A137
Lusso, E., Comastri, A., Simmons, B. D., et al. 2012, MNRAS, 425, 623
Magorrian, J., Tremaine, S., Richstone, D., et al. 1998, AJ, 115, 2285
Małek, K., Buat, V., Roehlly, Y., et al. 2018, A&A, 620, A50
Marconi, A., & Hunt, L. K. 2003, ApJ, 589, L21
Masoura, V. A., Mountrichas, G., Georgantopoulos, I., et al. 2018, A&A, 618, A31
Masoura, V. A., Mountrichas, G., Georgantopoulos, I., & Plionis, M. 2021, A&A, 646, A167
McMahon, R. G., Banerji, M., Gonzalez, E., et al. 2013, The Messenger, 154, 35
Menzel, M.-L., Merloni, A., Georgakakis, A., et al. 2016, MNRAS, 457, 110
Merloni, A., Bongiorno, A., Bolzonella, M., et al. 2010, ApJ, 708, 137
Mountrichas, G. 2023, A&A, 672, A98
Mountrichas, G., & Shankar, F. 2023, MNRAS, 518, 2088
Mountrichas, G., Georgakakis, A., & Georgantopoulos, I. 2019, MNRAS, 483, 1374
Mountrichas, G., Buat, V., Georgantopoulos, I., et al. 2021a, A&A, 653, A70
Mountrichas, G., Buat, V., Yang, G., et al. 2021b, A&A, 646, A29
Mountrichas, G., Buat, V., Yang, G., et al. 2021c, A&A, 653, A74
Mountrichas, G., Buat, V., Yang, G., et al. 2022a, A&A, 663, A130
Mountrichas, G., Masoura, V. A., Xilouris, E. M., et al. 2022b, A&A, 661, A108
Mukai, K. 1993, Legacy, 3, 21
Mullaney, J. R., Alexander, D. M., Aird, J., et al. 2015, MNRAS, 453, L83
Park, T., Kashyap, V. L., Siemiginowska, A., et al. 2006, ApJ, 652, 610
Pierre, M., Pacaud, F., Adami, C., et al. 2016, A&A, 592, A1
Pineau, F. X., Derriere, S., Motch, C., et al. 2017, A&A, 597, A28
Piotrowska, J. M., Bluck, A. F. L., Maiolino, R., & Peng, Y. 2022, MNRAS, 512, 1052
Poitevineau, R., Castignani, G., & Combes, F. 2023, A&A, 672, A164
Pouliasis, E., Mountrichas, G., Georgantopoulos, I., et al. 2020, MNRAS, 495, 1853
Pouliasis, E., Mountrichas, G., Georgantopoulos, I., et al. 2022, A&A, 667, A56
Rosario, D. J., Trakhtenbrot, B., Lutz, D., et al. 2013, A&A, 560, A72
Santini, P., Rosario, D. J., Shao, L., et al. 2012, A&A, 540, A109
Scodeggio, M., Guzzo, L., Garilli, B., et al. 2018, A&A, 609, A84
Setoguchi, K., Ueda, Y., Toba, Y., & Akiyama, M. 2021, ApJ, 909, 188
Shen, Y., & Liu, X. 2012, ApJ, 753, 125
Shen, Y., Greene, J. E., Strauss, M. A., Richards, G. T., & Schneider, D. P. 2008, ApJ, 680, 169
Shen, Y., Richards, G. T., Strauss, M. A., et al. 2011, ApJS, 194, 45
Shen, Y., McBride, C. K., White, M., et al. 2013, ApJ, 778, 98
Shimizu, T. T., Mushotzky, R. F., Meléndez, M., Koss, M., & Rosario, D. J. 2015, MNRAS, 452, 1841
Shimizu, T. T., Mushotzky, R. F., Meléndez, M., et al. 2017, MNRAS, 466, 3161
Sobral, D., Smail, I., Best, P. N., et al. 2013, MNRAS, 428, 1128
Stalevski, M., Fritz, J., Baes, M., Nakos, T., & Popović, L. Č. 2012, MNRAS, 420, 2756
Stalevski, M., Ricci, C., Ueda, Y., et al. 2016, MNRAS, 458, 2288
Stanley, F., Harrison, C. M., Alexander, D. M., et al. 2015, MNRAS, 453, 591
Sun, M., Trump, J. R., Brandt, W. N., et al. 2015, ApJ, 802, 14
Suh, H., Civano, F., Trakhtenbrot, B., et al. 2020, ApJ, 889, 32
Sutherland, W., & Saunders, W. 1992, MNRAS, 259, 413
Taylor, M. B. 2005, in Astronomical Data Analysis Software and Systems XIV, eds. P. Shopbell, M. Britton, & R. Ebert, ASP Conf. Ser., 347, 29
Tremaine, S., Gebhardt, K., Bender, R., et al. 2002, ApJ, 574, 740
Villa-Velez, J. A., Buat, V., Theule, P., Boquien, M., & Burgarella, D. 2021, A&A, 654, A153
Wright, E. L., Eisenhardt, P. R. M., Mainzer, A. K., et al. 2010, AJ, 140, 1868
Yang, G., Chen, C. T. J., Vito, F., et al. 2017, ApJ, 842, 72
Yang, G., Boquien, M., Buat, V., et al. 2020, MNRAS, 491, 740
Yang, G., Boquien, M., Brandt, W. N., et al. 2022, ApJ, 927, 192